AB

Katholieke *Universiteit* Nijmegen

Nijmegen-preprint
HEN-373
April 1996

Nuclear-Target Diffraction Dissociation in π^+ and K^+ Collisions with Au and Al at 250 GeV/*c*

EHS/NA22 Collaboration

CERN LIBRARIES, GENEVA
SCAN-9606059

SW9624

Nijmegen-preprint
HEN-373
April 1996

Nuclear-Target Diffraction Dissociation in π^+ and K^+ Collisions with Au and Al at 250 GeV/c

EHS/NA22 Collaboration

N.M. Agababyan[7], M.R. Atayan[7], M. Charlet[4,a], E.A. De Wolf[1,b], K. Dziunikowska[2,c], A.M.F. Endler[5], Z.Sh. Garutchava[6,d], H.R. Gulkanyan[7], R.Sh. Hakobyan[7], J.K. Karamyan[7], D. Kisielewska[2,c], W. Kittel[4], S.S. Mehrabyan[7], Z.V. Metreveli[6], K. Olkiewicz[2,c], F.K. Rizatdinova[3], E.K. Shabalina[3], L.N. Smirnova[3], M.D. Tabidze[6], L.A. Tikhonova[3], A.V. Tkabladze[6], A.G. Tomaradze[6], F. Verbeure[1], S.A. Zotkin[3]

[1] Department of Physics, Universitaire Instelling Antwerpen, B-2610 Wilrijk , Belgium
[2] Institute of Physics and Nuclear Techniques of the Academy of Mining and Metallurgy and Institute of Nuclear Physics, PL-30055 Krakow, Poland
[3] Nuclear Physics Institute, Moscow State University, RU-119899 Moscow, Russia
[4] High Energy Physics Institute Nijmegen (HEFIN), University of Nijmegen/NIKHEF, NL-6525 ED Nijmegen, The Netherlands
[5] Centro Brasileiro de Pesquisas Fisicas, BR-22290 Rio de Janeiro, Brazil
[6] Institute for High Energy Physics of Tbilisi State University, GE-380086 Tbilisi, Georgia
[7] Institute of Physics, AM-375036 Yerevan, Armenia

Abstract. An analysis of the A-dependence of the target-diffractive cross-section is presented. Data on the t-dependence of the cross section are fitted in the usual exponential form. The mean multiplicity of negative particles produced diffractively is found not to be sensitive to the nuclear mass. The A-dependence of the emitted proton multiplicity and the angular distributions of the produced charged particles suggest re-scattering of the emitted particles on other nucleons of the nucleus. All these facts are compared with results obtained by Monte-Carlo simulation according to a two-component Dual Parton Model.

---

[a] EC guest scientist, now at DESY, Hamburg
[b] Onderzoeksleider NFWO, Belgium
[c] Supported by the Polish State Committee for Scientific Research
[d] Now at UIA, Wilrijk, Belgium

1 Introduction

Coherent excitation of hadrons by nuclei leaving the nucleus undisturbed, has been studied in a number of experiments [1-8]. Nuclear target diffraction dissociation, on the other hand, is scarcely studied, both experimentally and theoretically. This, in spite of the fact that such a process could give clues about the parton structure of nucleons inside the nucleus or on the dynamics of Pomeron interaction with nuclear matter.

So far, the only published experimental work comes from the HELIOS Collaboration [9]. It concerns diffraction dissociation of Be, Al and W targets excited by a proton beam of 450 GeV/c. The results suggest that the dominant process of nuclear diffractive excitation is the dissociation of single nucleons. Recently, numerical estimates [10] based on multiple-scattering theory have been compared with the HELIOS data.

In this paper, for the first time an analysis is presented of diffraction dissociation of Au and Al targets excited by a meson beam. This is performed in the NA22 experiment by means of a positive, meson enriched beam of 250 GeV/c. NA22 data have been collected both for hadron-hadron and hadron-nucleus collisions to allow a comparison under the same experimental conditions.

The paper is organized as follows: The experimental procedure is described in Sect. 2. The model description is shortly presented in Sect. 3. The results are presented in Sect. 4 and discussed in Sect. 5.

2 Experimental procedure

The data have been collected with the European Hybrid Spectrometer (EHS) at the CERN Super-Proton Synchrotron (SPS) by the NA22 collaboration. The experimental set-up of the EHS is described in detail elsewhere [11]. A Rapid Cycling Bubble Chamber (RCBC) filled with hydrogen and equipped with two nuclear targets consisting of an aluminium and a gold foil with thickness of 2.5 mm and 0.64 mm, respectively, corresponding to 0.5% of an interaction length, has been used as a target and a vertex detector simultaneously. Thus, interactions with hydrogen as well as with Al and Au nuclei have been detected in a single experiment. As a vertex detector, the RCBC provided a good tool to use ionization measurements to identify slow charged particles, mainly recoil protons, with laboratory momentum up to 1.2 GeV/c.

The selection criteria for the event and track sample are described in detail in our earlier paper [12]. They can be summarized as follows:

1. The beam track is well measured and reconstructed;
2. the interaction vertex is within one of the nuclear foils;
3. the loss of tracks due to measurement or reconstruction failures is limited in number, depending on the event topology;
4. the event is not a candidate for an elastic or coherent interaction with the nucleus.

In order to compensate for losses due to item 3, tracks are weighted depending on the charge of the track and the topology of the event and events are weighted with a multiplicity dependent weight. Futhermore, each event is weighted to correct for losses induced by the interaction trigger [13]. This weight depends strongly on the spatial characteristics of the event. It is determined for each reconstructed event from the overall azimuthal symmetry around the beam axis. The mean value of the trigger weights used in the interval $0.1 > -t > 0.025$ GeV^2 is 2.29. We restrict the analysis to the squared four-momentum transfer region $-t > 0.025$ GeV^2 due to the trigger bias in the very small $-t$ region.

A total of 2521 K^+ and 7487 π^+ candidate interactions with Al and Au are submitted to the above criteria and result in a sample of 4905 π^+/K^+ interactions with Al and 4155 π^+/K^+ with Au. To

select for diffraction dissociation, the same cuts are imposed as for our earlier investigation of target diffraction in $\pi^+/\mathrm{K}^+\mathrm{p}$ interactions in the same experiment [14]. They are:

1. The secondary particle with the highest value of the Feynman variable x_F must be a positive (π^+ or K^+) particle and x_F must be larger than 0.8.
2. The rapidity gap between the largest x_F particle and its nearest charged neighbour is required to be the largest in the event and must be larger than 2.0 units.

These cuts are tested in diffractive Monte-Carlo events and the efficiencies of these cuts are estimated as 94% for Al and 96% for Au.

By these cuts, the sample is reduced to 177 π^+/K^+Al and 132 π^+/K^+Au interactions. We investigate this limited sample and compare our results with those of HELIOS and with the expectations from a Monte-Carlo model.

3 Model description

For comparison with our data, we use the DTUNUC code [15] to generate 4000 Monte-Carlo π^+Al, K^+Al, π^+Au and K^+Au interactions. This code can produce single target-diffractive hadron-nucleus interactions within the framework the Dual Parton Model [16], when the incoming hadron only undergoes one interaction with the nucleus. We work with 880 π^+/K^+Al and 440 π^+/K^+Au diffractive events that have survived the same cuts as applied to the experimental data.

In DTUNUC, single-diffractive hadron-nucleus interactions are treated as Glauber processes involving one single target nucleon only. The fraction $\sigma_\mathrm{TD}/\sigma^n_\mathrm{inel}$ of these collisions is diffractive, where σ_TD is the hadron-nucleon target-diffraction cross-section and σ^n_inel is the inelastic hadron-nucleon cross-section.

Using DPM to generate Monte Carlo events, the particle production is obtained by the fragmentation of colorless parton-parton chains constructed from the quark content of the interacting hadrons. The hadronization of single chains is handled by the fragmentation model BAMJET [17]. Fermi momenta of nucleons within the interacting nucleus are considered, together with a simple realization of the Pauli principle.

The cascade of secondaries generated in the target nucleus is taken in account. This mechanism contributes significantly to particle production in the target fragmentation region. The transverse momentum p_T of the produced particles and the invariant mass M_X of the diffractive system are sampled from an exponential p_T distribution and a $1/M^2_\mathrm{X}$ distribution, respectively. The decay of resonances is handled by the code DECAY [18].

The same model has been applied to target diffraction of Beryllium, Aluminium and Tungsten by protons at 450 GeV [19] and compared with data of the HELIOS collaboration [9]. The single-diffractive cross sections calculated with the model are larger than the values obtained by HELIOS. Difficulties also arise to reproduce the average multiplicities and the slopes presented by the HELIOS collaboration.

4 Experimental Results

In Fig. 1 we present the x_F distribution ($x_\mathrm{F} > -0.05$) of the fastest positively charged hadron for all events (before the application of cuts) grouped in different topologies and targets (unshaded histograms). To suppress the non-diffractive background, the rapidity-gap cut as described in Sect. 2 is applied (shaded histograms). As can be seen from the figure, this leads to a drastic reduction of the non-diffractive background at $x_\mathrm{F} < 0.8$, but leaves the leading-particle signal almost unchanged. We interpret the signal of the fastest positively charged hadron after these cuts (rapidity-gap >2 and

$x_F > 0.8$) as mainly originating from diffraction dissociation of the nucleus. The remaining non-diffractive background under the leading-particle signal is approximated by a smooth hand-drawn curve extrapolating the x_F-spectra from $x_F < 0.8$ to $x_F = 1$ (lines in Fig. 1). It is suppressed in what follows by a multiplicity and x_F dependent weight calculated for each event, such as to reproduce the x_F distribution of the fastest positive hadron (Fig. 1) after subtraction of the background.

In Figs. 2a and 2b, the distribution in the Feyman variable x_F is shown for the most energetic beam-like secondary particle produced in target-diffractive events, together with the particles from diffraction dissociation of the Al and Au nuclei, respectively. The full- and dashed-line histograms are normalized to the sum N_{ev} of weighted diffractive events ($-t > 0.025$ GeV^2) and represent the experimental and Monte Carlo data, respectively. One can see that the beam-like particle is well separated from the dissociation products of the diffractively produced system. A long tail is found in the backward region where identified protons are shown as grey histogram. This tail is more prominent for Au than for Al. It is a first hint that emitted particles suffer re-scattering from other nucleons of the nucleus.

4.1 Cross sections

The differential distribution $(1/N_{ev})(dN_{ev}/dt)$ is shown in Figs.3a and 3b for Al and Au, respectively. In this case, N_{ev} is the sum of weighted diffractive events with $0.025 < -t < 1.025$ GeV^2. Again, the full and dashed lines represent experimental data and Monte-Carlo predictions, respectively. Experimental data and model predictions are fitted by exponentials of the form

$$dN_{ev}/dt \propto e^{-b|t|} \ . \tag{1}$$

The values obtained for the slope parameters b are given in Table 1. In the model, the slope parameter b is somewhat overestimated as compared to the value obtained from the experimental data. The slopes are smaller than those found by HELIOS with a diffractive cut of $x_F > 0.925$ in the range $0.01 \leq -t \leq 0.36$ GeV^2 (7.62±0.62 for Al and 7.91±0.47 for W). Applying the HELIOS x_F-cut to our Al data and reducing the fit range to $0.025 < -t < 0.325$ GeV^2, the value changes to 5.5±2.0 and 2.9±2.2 for Al and Au, respectively. The difference observed between the slope parameter for meson-induced and proton-induced target-diffraction reactions reflects the different t dependence of meson-pomeron (meson-reggeon) and proton-pomeron (proton-reggeon) couplings.

The target-diffraction cross-sections for π^+/K^+Al and for π^+/K^+Au are obtained from the differential cross sections dN_{ev}/dt by an extrapolation over the remaining part of the t region by means of the exponential fits shown in Figs.3a and 3b and multiplication by the μb-equivalent σ_{inel}/N_{inel} for inelastic events. The inelastic cross section σ_{inel} has been obtained by an interpolation over published data between 60 and 280 GeV/c [20]. The following values for the cross-sections are found:

$$\sigma_{TD}(\mathrm{Al}) = 10.3 \pm 3.1\mathrm{mb} \text{ and } \sigma_{TD}(\mathrm{Au}) = 40.1 \pm 14.2\mathrm{mb} \ .$$

The A-dependence of the integrated diffractive cross-section is shown in Fig. 4, where also our target-diffractive cross-section for π^+/K^+p [14] is included. If we assume the conventional parameterization $\sigma_{TD} \propto A^\alpha$ we find

$$\alpha = 0.58 \pm 0.06.$$

The HELIOS collaboration [9] has obtained $\alpha = 0.35 \pm 0.02$ for proton-nucleus data. With the assumption described in Sect. 3, the Glauber model indeed predicts an A-dependence stronger for meson-nucleus than for proton-nucleus target diffraction dissociation. In this model, different values of α are expected from the difference in the cross sections for the elementary inelastic interactions.

Within the large errors and possible biases of both experiments, we can conclude that both results are consistent with the assumption that target diffraction occurs on only one single nucleon.

4.2 *Mass dependence*

In Figs. 5a and 5b we show, both for the experimental data and Monte-Carlo, the distribution in the squared invariant mass M_X^2 of the diffractive system, calculated assuming that the nucleon is at rest before the interaction. The distribution is normalized to the sum of weighted events with $1 \leq M_X \leq 10$ GeV. As indicated by the straight lines, the distribution is in good agreement with the characteristic $1/M_X^2$ dependence of the diffractive cross section.

The average multiplicity $\langle n \rangle$ of charged particles of the diffractive system is shown as a function of M_X in Figs. 6a and 6b. Both sub-figures exhibite the usual steady increase of $\langle n \rangle$ with increasing M_X. This trend is followed by the model, but the mean multiplicity of the Monte-Carlo events (dashed lines) is smaller than that observed experimentally (full lines). Table 2 gives the values obtained for the average charge, positive, negative and proton multiplicity, both for experimental data and Monte-Carlo simulations. In the experimental data, the mean positive and proton multiplicities are larger for Au than for Al and only the mean negative multiplicity does not depend on A. A plausible physical explanation of this observation is re-scattering inside the nucleus. The difference of the mean positive multiplicity between Monte-Carlo predictions and data indicates that the process of cascading is underestimated in the model.

The normalized p_T distribution $(1/N)\mathrm{d}N/\mathrm{d}p_T^2$ of the diffractively produced particles, integrated over all masses M_X of the diffractively produced system and normalized to the sum of weighted tracks with $p_T < 2.4$ GeV/c, is given in Figs. 7a and 7b for Al and Au nuclei, respectively. It shows an exponential behavior,

$$\mathrm{d}N/\mathrm{d}p_T^2 \propto e^{-Bp_T}\,, \tag{2}$$

with slope B as given in the right part of table 1. The average transverse momentum $\langle p_T \rangle$ can be determined from the slope parameter as $\langle p_T \rangle = 2/B$. The result for the experimental data is $\langle p_T \rangle = 340 \pm 7$ MeV for Al and $\langle p_T \rangle = 318 \pm 7$ MeV for Au.

4.3 *The dissociation of the diffractively produced system*

In Figs. 8a and 8b, the distribution of particles emitted from the diffractively produced system is shown in terms of their Feynman variable x_{FX} in the cms of the excited nucleon. This and the following distributions are normalized to the sum of weighted tracks. The distributions [experimental (full lines) and Monte-Carlo (dashed lines)], show an asymmetry more accentuated for Au than for Al, with more particles produced in the backward hemisphere. Such an effect is expected when intranuclear cascading occurs, as is already suggested by the observations from Fig. 2 and Table 2. While for Al experimental data and Monte-Carlo show a similar distribution for the backward particles, the experimental data for Au show relatively more backward particles than the Monte-Carlo results.

To study the dissociation of the diffractively produced system in more detail, the normalized angular distribution of charged particles in the cms of the excited nucleon is given in Figs. 9a and 9b. It shows a longitudinal form of the internal structure of the diffractive system. Again, the data show forward-backward asymmetry with more particles produced in the backward hemisphere. To investigate which kind of charged particle is responsible for this asymmetry, Figs. 10a and 10b give the normalized angular distribution for negative particles. The experimental angular distribution is approximately symmetric and agrees very well with the Monte-Carlo results. We can conclude that the positively charged particles (probably mainly due to protons) give the main contribution to the asymmetry observed in Fig. 9. This fact can indeed be explained from a significant re-scattering of the emitted particles with other protons of the nucleus.

5 Conclusions

We have investigated the diffractive excitation of Al and Au nuclei by a beam of π^+/K^+ mesons at 250 GeV/c. The A-dependence of the target-diffractive cross section can be parameterized as A^α, where $\alpha = 0.58 \pm 0.06$, considerably larger than observed for incident protons. The transverse momentum distribution follows an exponential and the mass spectrum of the diffractively produced system follows a $1/M_X^2$ dependence. These results indicate that target diffraction occurs on only one single nucleon of the nucleus. However, the abundance of positive particles emitted in the backward direction indicates that there must be re-scattering of the emitted particles on other nucleons of the nucleus.

The Monte-Carlo simulation according to the DTUNUC code gives reasonable agreement with the data for transverse momentum and mass dependence, but the cascade generated in the target nucleus is insufficient to reproduce the experimental multiplicity of the diffractive system.

Furthermore, the slope parameter b of the differential distribution in the squared four-momentum transfer is overestimated in the model.

Acknowledgements

We are grateful to the III. Physikalisches Institut B, RWTH Aachen, Germany, the DESY-Institut für Hochenergiephysik, Berlin-Zeuthen, Germany, the Department of High Energy Physics, Helsinki University, Finland, the Institute for High Energy Physics, Protvino, Russia, and the University of Warsaw and Institute of Nuclear Problems, Warsaw, Poland for early contributions to this experiment. This work is part of the research programme of the "Stichting voor Fundamenteel Onderzoek der Materie (FOM)", which is financially supported by the "Nederlandse Organisatie voor Wetenschappelijk Onderzoek (NWO)". We further thank NWO for support of this project within the program for subsistence to the former Soviet Union (07-13-038).

References

1. C. Bemporad et al.: Nucl. Phys. B33 (1971) 397.
2. C. Bemporad et al.: Nucl. Phys. B42 (1972) 627.
3. P. Mühlemann et al.: Nucl. Phys. B59 (1973) 106.
4. W. Beush et al.: Phys. Lett. 55B (1975) 97.
5. T.J. Roberts et al.: Phys. Rev. D18 (1978) 59.
6. G. Bellini et al.: Nucl. Phys. B199 (1982) 1.
7. M. Zielinski et al.: Z. Phys. C16 (1983) 197.
8. N.M. Agababyan et al. (NA22 Coll.): "Coherent inelastic interactions of π^+ and K^+-mesons on Al and Au nuclei at 250 GeV/c", Nijmegen preprint HEN-374 (1995), Z. Phys. C (1996), in print.
9. T. Åkesson et al.: Z. Phys. C49 (1991) 355.
10. V.R. Zoller: Nucl. Phys.B (Proc. Suppl.) 25B (1992) 110.
11. M. Aguilar-Benitez et al.: Nucl. Inst. Methods 205 (1983) 79.
12. I.V. Ajinenko et al. (NA22 Coll.): Z. Phys. C42 (1989) 377.
13. M. Adamus et al. (NA22 Coll.): Z. Phys. C32 (1986) 475.
14. M. Adamus et al. (NA22 Coll.): Z. Phys. C39 (1988) 301.
15. H. J. Moehring, J. Ranft: Z. Phys. C52(1991) 643; S. Roesler, R. Engel, J. Ranft: Z. Phys. C59 (1993)481.
16. A. Capella, U. Sukhatme, C.I. Tan and J. Tran Thanh Van, Orsay Preprint, LPTHE-92-38.
17. S. Ritter, J. Ranft: Acta Phys. Pol. B11 (1980) 259.
18. K. Häussgen and S. Ritter: Comp. Phys. Commun. 31 (1984) 411.
19. J. Ranft and S. Roesler: Z. Phys. C62 (1994) 329.
20. A.S. Carroll et al.: Phys. Lett. B80 (1979) 319.

Table 1. Slope parameters b of (1) and B of (2)

target	b (GeV^{-2}) $0.025 < -t < 0.525$ GeV^2		B (GeV^{-1}) $0 < p_{\mathrm{T}} < 2.4$ GeV/c	
	experiment	model	experiment	model
Al	3.9± 0.8	5.7±0.3	5.87±0.11	6.83±0.07
Au	3.9± 1.0	5.4±0.4	6.27±0.14	6.47±0.08

Table 2. Average charge, positive, negative and proton multiplicity

target	Average charge multiplicity		Average positive multiplicity	
	experiment	model	experiment	model
Al	4.81± 0.25	3.58±0.07	3.08±0.16	2.28±0.04
Au	5.84± 0.47	3.83±0.12	4.07±0.35	2.38±0.08
target	Average negative multiplicity		Average proton multiplicity	
	experiment	model	experiment	model
Al	1.73± 0.10	1.30±0.03	0.99±0.10	0.93±0.03
Au	1.77± 0.15	1.45±0.05	1.82±0.22	0.98±0.06

Figure Captions

Fig. 1 The x_{F} spectrum of the fastest positive hadron for different multiplicities and targets, without cuts (unshaded area) and after the maximum-rapidity-gap cut (shaded area). Arrows indicate the x_{F} cut for the selection of diffractive events; lines under the large-x_{F} signals are estimated background.

Fig. 2 The normalized x_{F} distribution of particles produced in interactions on Al and Au, respectively. Full lines represent the experimental distribution and dashed lines represent the DTM Monte-Carlo distribution. The shaded histogram represents protons identified in the experimental data.

Fig. 3 The normalized t distributions for target-diffractive π^+/K^+ interactions on Al and Au. Lines as in Fig. 2.

Fig. 4 The A-dependence of the integrated target-diffractive cross-section for π^+/K^+ interactions on p, Al and Au.

Fig. 5 The normalized M_{X}^2 distributions compared to a $1/M_{\mathrm{X}}^2$ dependence. Lines as in Fig. 2.

Fig. 6 The average multiplicity $\langle n \rangle$ of charged particles as a function of M_{X}. Lines as in Fig. 2.

Fig. 7 The normalized transverse momentum distribution. Lines as in Fig. 2.

Fig. 8 The normalized Feynman x_{FX} distribution of particles emitted from the diffractively produced system in the cms of the excited nucleon. Lines as in Fig. 2.

Fig. 9 The normalized angular distribution of the charged particles in the cms of the excited nucleon. Lines as in Fig. 2.

Fig. 10 As Fig. 9, but for negative particles.

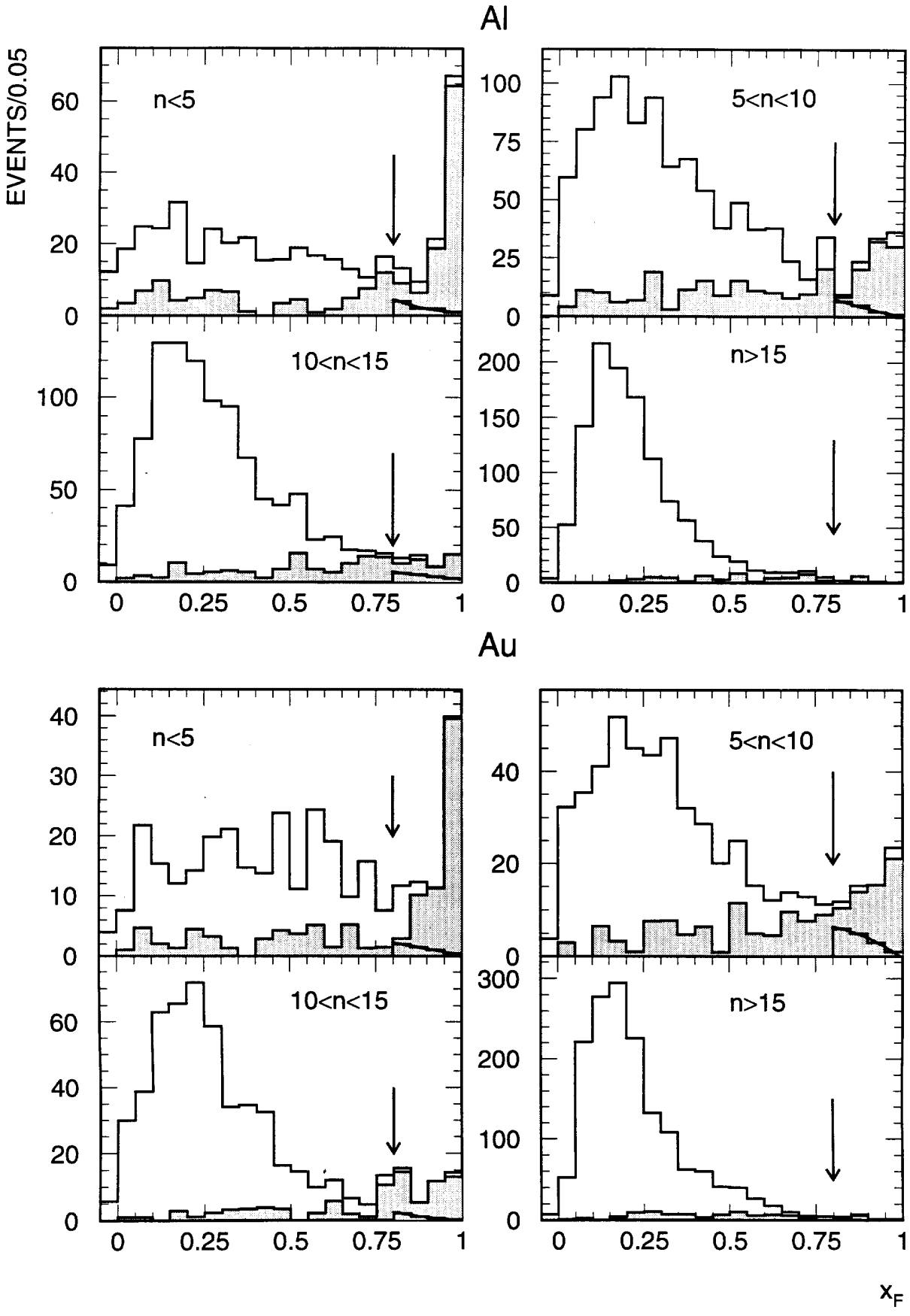

Fig. 1

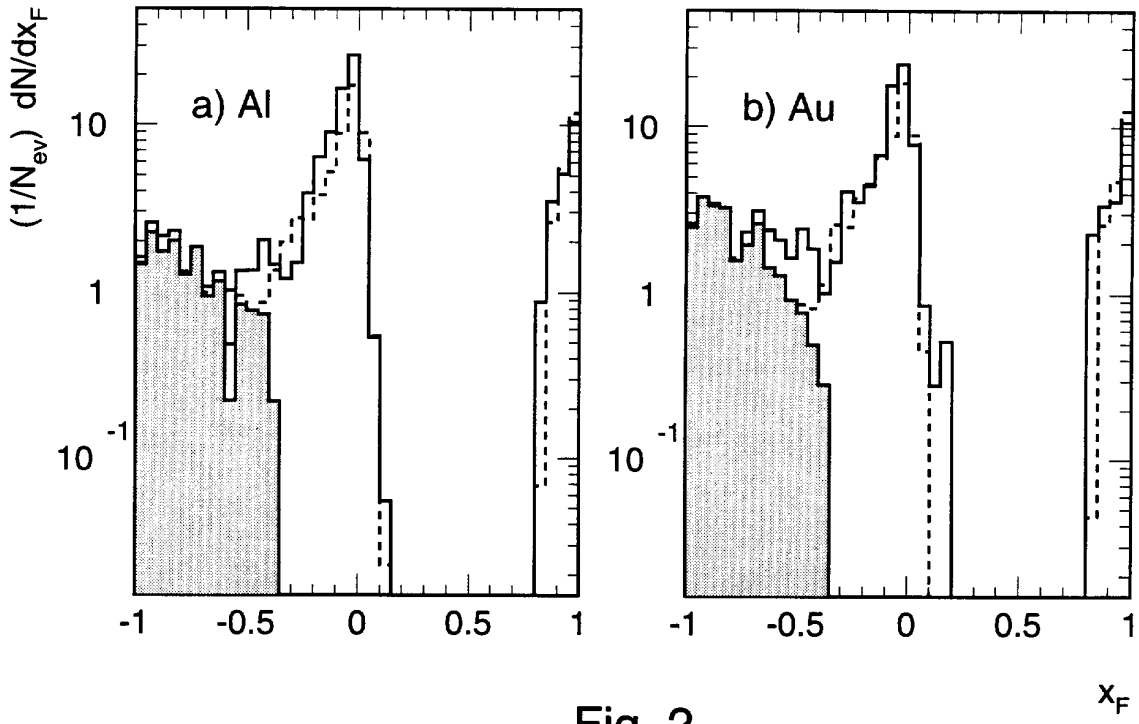
(1/N_ev) dN/dx_F
a) Al
b) Au
10
1
10^-1
-1
-0.5
0
0.5
1
x_F

Fig. 2

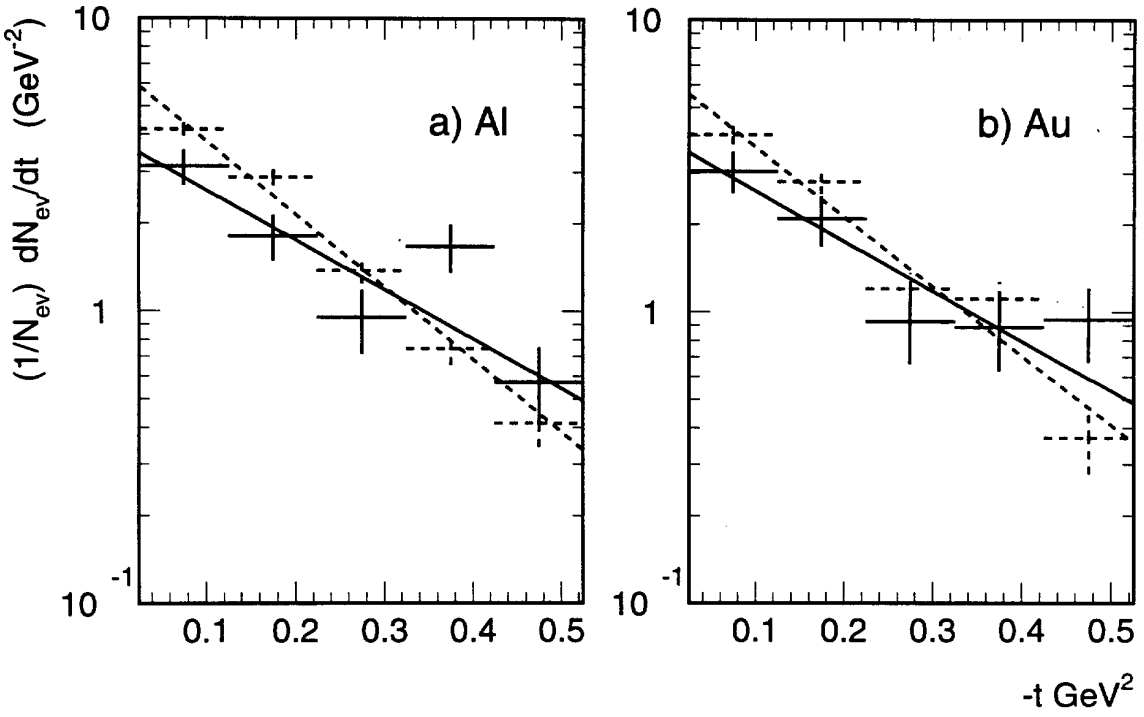
(1/N_ev) dN_ev/dt (GeV^-2)
a) Al
b) Au
10
1
10^-1
0.1
0.2
0.3
0.4
0.5
-t GeV^2

Fig. 3

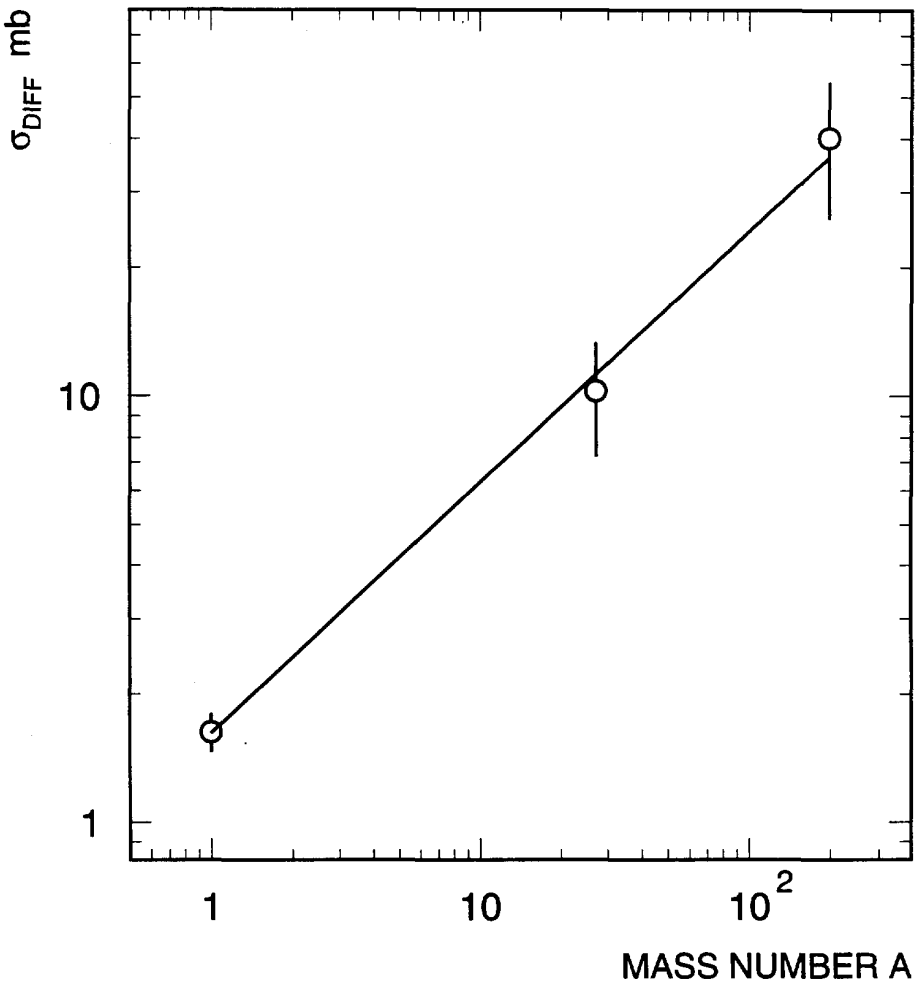

Fig. 4

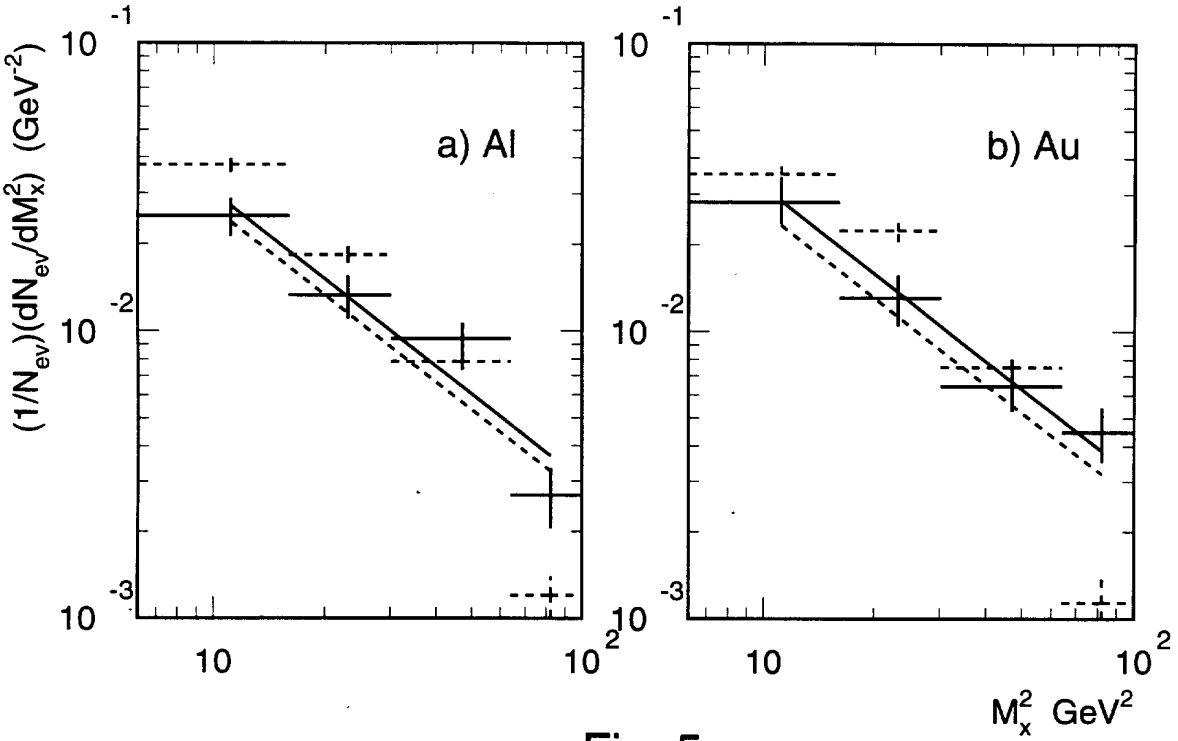
a) Al
b) Au
$(1/N_{ev})(dN_{ev}/dM_x^2)$ (GeV^{-2})
M_x^2 GeV^2

Fig. 5

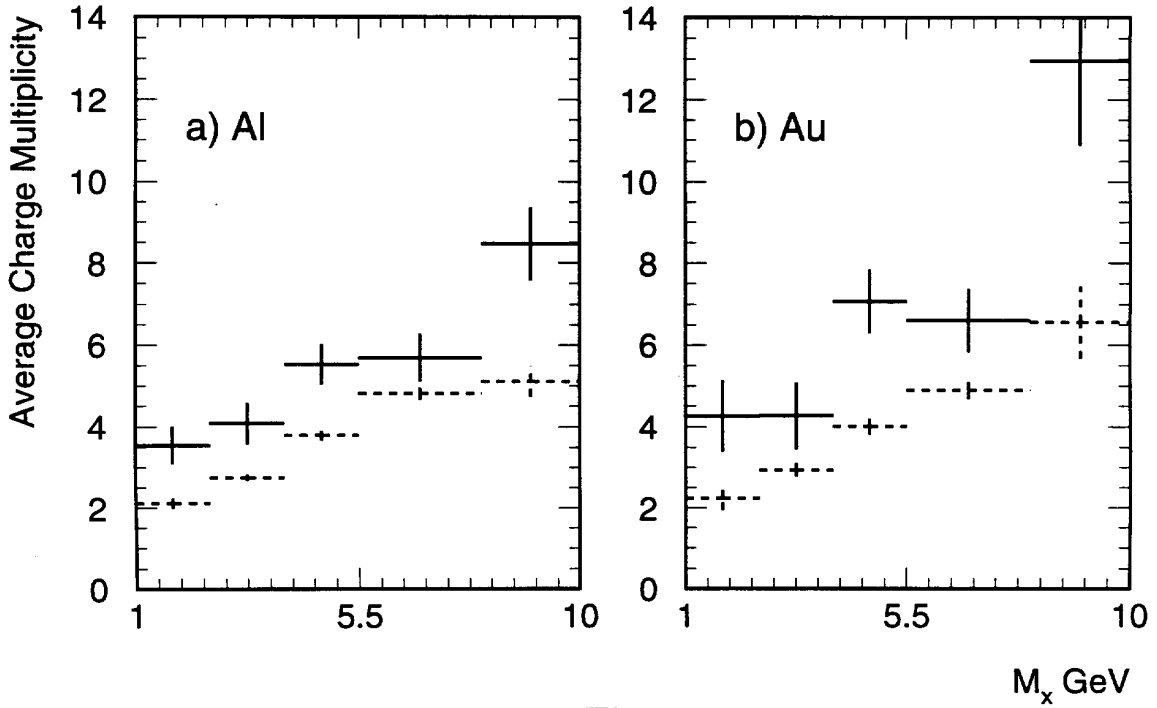
a) Al
b) Au
Average Charge Multiplicity
M_x GeV

Fig. 6

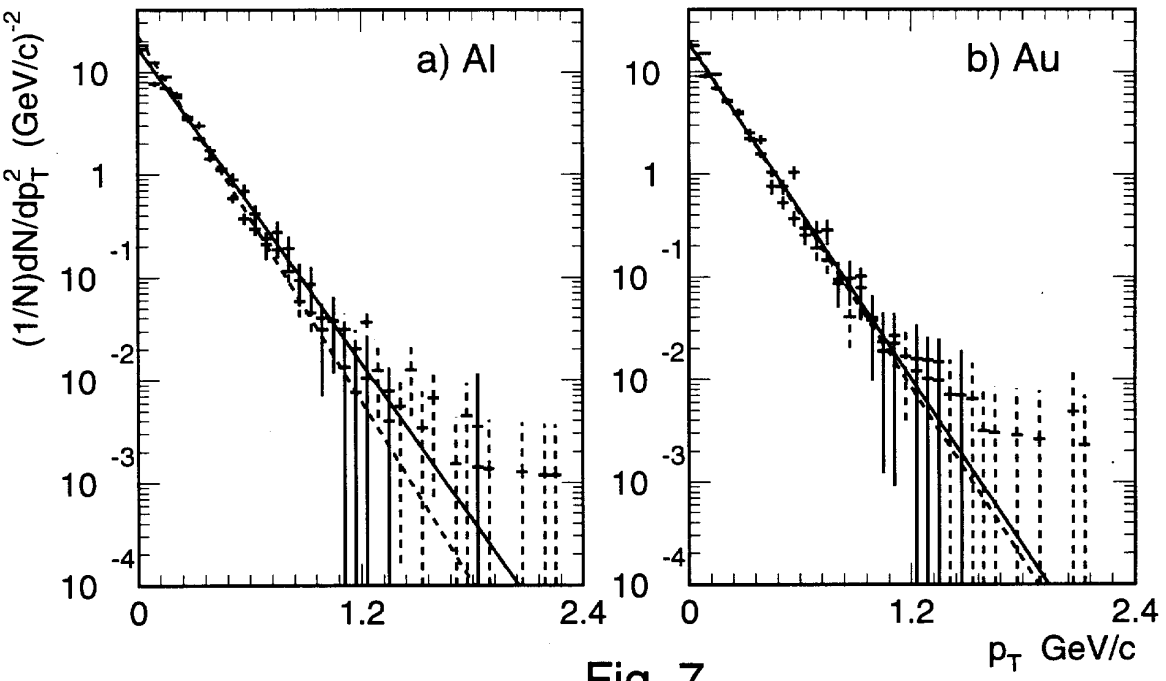

Fig. 7

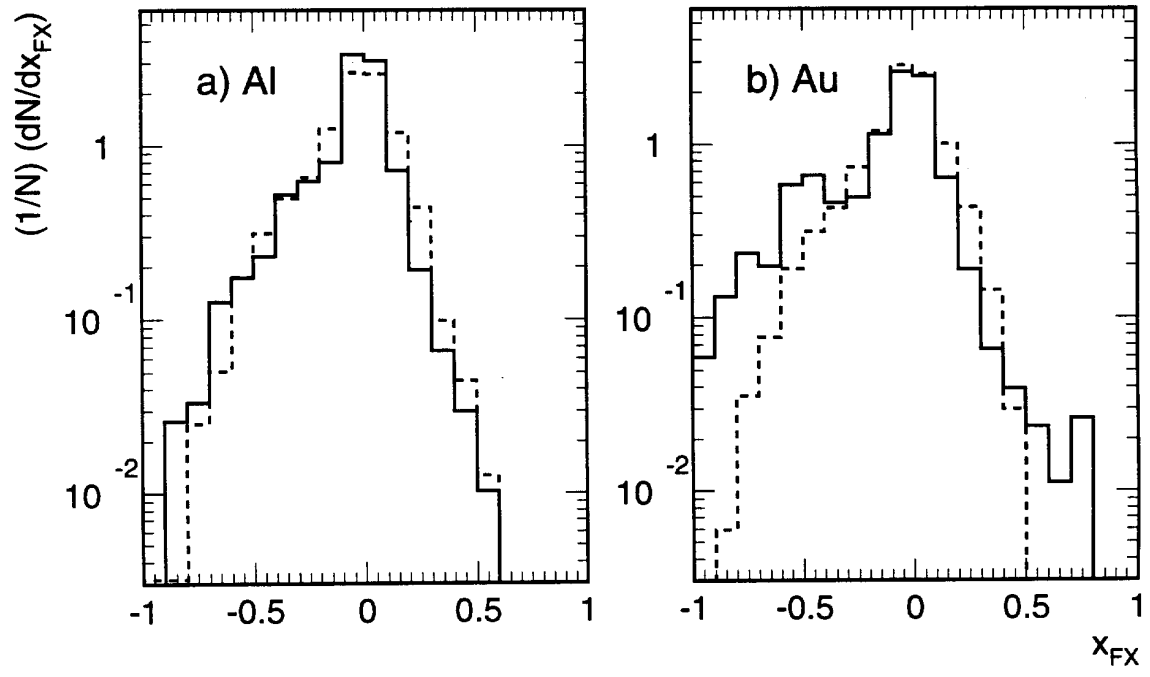

Fig. 8

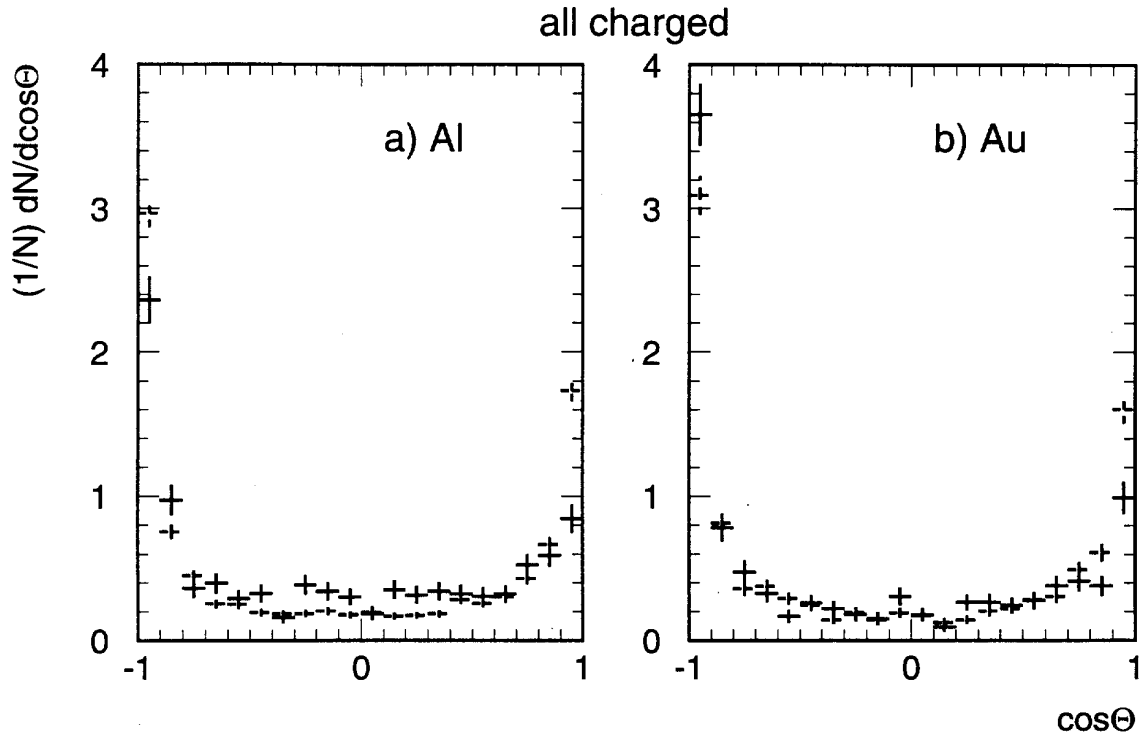
all charged
(1/N) dN/dcosΘ
a) Al
b) Au
cosΘ

Fig.9

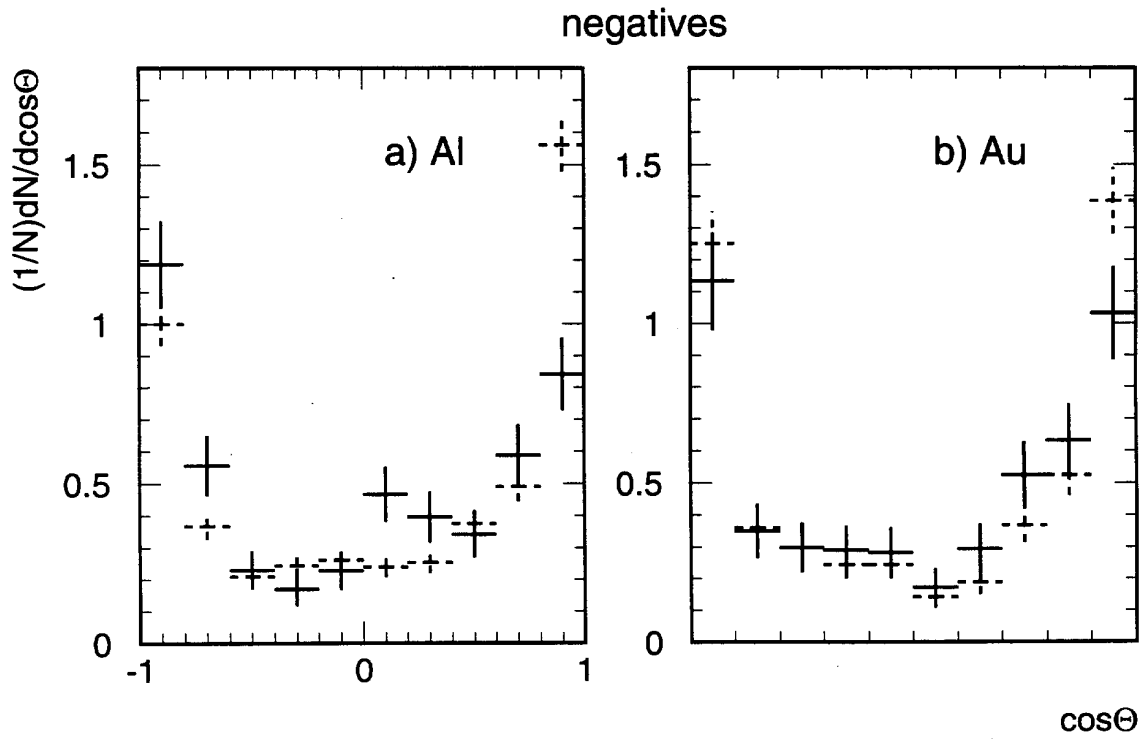
negatives
(1/N)dN/dcosΘ
a) Al
b) Au
cosΘ

Fig.10